# PROCEEDINGS OF SPIE

SPIEDigitalLibrary.org/conference-proceedings-of-spie

# Subwavelength antimonide infrared detector coupled with dielectric resonator antenna

Kazemi, Alireza, Shu, Qingyuan, Dahiya, Vinita, Taghipour, Zahra, Paradis, Pablo, et al.

Alireza Kazemi, Qingyuan Shu, Vinita Dahiya, Zahra Taghipour, Pablo Paradis, Christopher Ball, Theodore J. Ronningen, Stefan Zollner, Steven M. Young, Jordan Budhu, Kevin A. Grossklaus, Thomas E. Vandervelde, Anthony Grbic, Sanjay Krishna, "Subwavelength antimonide infrared detector coupled with dielectric resonator antenna," Proc. SPIE 11002, Infrared Technology and Applications XLV, 1100221 (7 May 2019); doi: 10.1117/12.2518807



Event: SPIE Defense + Commercial Sensing, 2019, Baltimore, Maryland, United States

# Subwavelength antimonide infrared detector coupled with dielectric resonator antenna

Alireza Kazemi<sup>a</sup>, Qingyuan Shu<sup>a</sup>, Vinita Dahiya<sup>a</sup>, Zahra Taghipour<sup>a</sup>, Pablo Paradis<sup>c</sup>, Christopher Ball<sup>d</sup>, Theodore J. Ronningen<sup>a</sup>, Stefan Zollner<sup>c</sup>, Steven M. Young<sup>b</sup>, Jordan Budhu<sup>b</sup>, Kevin A. Grossklaus<sup>e</sup>, Thomas E. Vandervelde<sup>e</sup>, Anthony Grbic<sup>b</sup>, Sanjay Krishna\*<sup>a</sup>

<sup>a</sup>Department of Electrical and Computer Engineering, The Ohio State University, 2015 Neil Avenue, Columbus, OH USA 43210; <sup>b</sup>Department of Electrical Engineering & Computer Science, University of Michigan, 1301 Beal Avenue, Ann Arbor, MI USA 48109; <sup>c</sup>Department of Physics, New Mexico State University, P.O. Box 30001, Las Cruces, NM USA 88003; <sup>d</sup>ElectroScience Laboratory, The Ohio State University, 1330 Kinnear Road, Columbus, OH USA 43212; <sup>e</sup>Department of Electrical and Computer Engineering, Tufts University, 161 College Avenue, Medford, MA USA 02155

## **ABSTRACT**

Antenna coupled detectors break the intrinsic tradeoff between signal and noise by "collecting over a large area" and "detecting over a small area". Most antenna coupled detectors in the infrared rely on a metal resonator structure. However, there are losses associated with metallic structures. We have demonstrated a novel long-wave infrared (LWIR) detector that combines a dielectric resonator antenna with an antimonide-based absorber. The detector consists of a 3D, subwavelength InAsSb absorber embedded in a resonant, cylindrical dielectric resonator antenna made of amorphous silicon. This architecture enables the antimonide detection element to shrink to deep subwavelength dimensions, thereby reducing its thermal noise. It is important to note that this concept only applies when (a) the detector noise is limited by bulk noise mechanisms with negligible surface leakage currents and (b) the dominant source of current in the device is due to dark current (such as diffusion) that scales with the volume of the detector. The dielectric resonator enhances the collection of photons with its resonant structure that couples incident radiation to the detector. We will present results on the absorption in structures with and without the dielectric resonator antenna. The signal to noise enhancement in the LWIR photodiodes integrated with the dielectric resonator antenna using radiometric characterization will be discussed.

Keywords: infrared, antennas, superlattice, antimonide, subwavelength, noise

# 1. INTRODUCTION

Thermal infrared sensing is widely used for a variety of purposes, including military, environmental, medical, and industrial applications. Sensors operating at long-wave infrared (LWIR) wavelengths, particularly traditional imagers and hyperspectral imagers, have matured rapidly over the past decade. Remote thermal imaging enables day/night surveillance of denied areas and can provide critical information on the operational state of facilities or vehicles, detection of camouflaged materiel, and characterization of natural disasters (wildfires, volcanoes, etc.). In addition, hyperspectral imaging enables detection of threat materials that have strong spectral absorption in the LWIR band, such as chemical warfare agents (especially nerve and blister agents), explosives, and toxic industrial chemicals.

Despite the ongoing development of increasingly capable LWIR sensors, there exists a need for enhanced sensor system technologies that facilitate operations in a resource-constrained environment. Current Mercury Cadmium Telluride (MCT-based) LWIR systems must be cooled, imposing an expensive and complicated logistical burden on satellite or aircraft operations. The development of LWIR detection technologies that do not require significant cooling infrastructure will substantially reduce operations cost and complexity. In addition, the proposed approach can lead to narrowband LWIR detectors. This opens the possibility of color-specific detectors without the added cost and complexity of optical components that spectrally resolve the incoming radiation.

\* krishna.53@osu.edu; phone 1 614 292-3715; fax 1 614 292-7596; kind.engineering.osu.edu

Infrared Technology and Applications XLV, edited by Bjørn F. Andresen, Gabor F. Fulop, Charles M. Hanson, Proc. of SPIE Vol. 11002, 1100221 © 2019 SPIE · CCC code: 0277-786X/19/\$18 · doi: 10.1117/12.2518807

Researchers at The Ohio State University and the University of Michigan have innovated a novel approach toward a high operating temperature LWIR detector. This Dielectric Resonator Antenna Coupled Antimonide Detector (DRACAD), shown schematically in Figure 1, combines a deep sub-wavelength antimonide detector with a dielectric resonator antenna (DRA). The small size of the detector reduces noise, which scales with the surface area of the detector, and the DRA provides impedance matching between the detector and impinging radiation, while also providing field enhancement within the antenna structure at the location of the detector element. There is a growing legacy of research involving infrared detectors coupled to structures such as antennas and gratings to enhance the detected signal. <sup>1-5</sup> Many of these studies focus primarily on metallic antennas and structures, not dielectric antennas that are the focus of the present investigation.

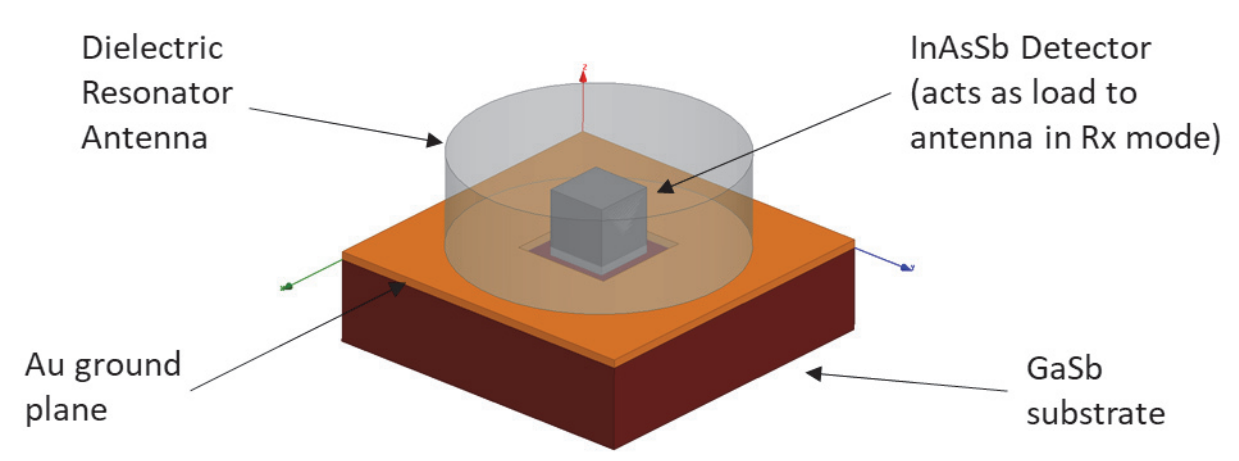


Figure 1. Schematic configuration of the DRACAD system, including a deep sub-wavelength antimonide detector atop a metallic ground plane and encased in a cylindrical dielectric resonator structure.

The remainder of this paper documents the development and testing of the DRACAD device. Section 2 provides background on the underlying phenomenology behind the antimonide detector and the dielectric antenna structure. Section 3 summarizes theoretical simulations intended to validate the DRACAD concept and to refine design choices for both the detector and antenna components. Section 4 describes the detector material growth and device fabrication process, followed by a description of preliminary optical testing in Section 5. Section 6 offers conclusions and a summary of next steps to continue the development and maturation of DRACAD technology.

#### 2. BACKGROUND

In order to understand how the combination of antimonide superlattice detector and dielectric resonator antenna can yield a high performance LWIR detector, one must first understand how each element functions on its own. This section summarizes key physical phenomena associated with the sensitivity of antimonide materials to LWIR radiation, scaling of noise with detector size, performance of dielectric resonator antennas compared to metal, and importance of impedance matching toward electric field concentration at the detector element.

Over the past decade or more, research has indicated that III-V semiconductors provide an optimal combination of lattice constant and bandgap energy to enable sensing over a broad range of infrared wavelengths. Materials with lattice constants near 6.1 Å, such as InAs, GaSb, and AlSb, provide effective sensing at wavelengths through the mid-wave infrared (MWIR).<sup>6-8</sup> In order to achieve detection at LWIR wavelengths, a lattice constant of 6.3 Å is desired, which can be achieved by InAs<sub>1-x</sub>Sb<sub>x</sub> matched to a virtual substrate of the same lattice constant.<sup>9-11</sup>

While great progress has been made in recent years toward the development of antimonide-based superlattice detectors, they still require cryogenic cooling for maximal signal-to-noise ratio (SNR) for operation at MWIR or LWIR wavelengths. In order to achieve higher operating temperatures, one must reduce the noise associated with these detectors. One way to do this is to shrink the size of the detector element. This concept only works when the dark current flowing in the device scales with the volume of the detector. For instance, if the detector is background limited or limited by the photon noise, then this concept will not lead to an increase in SNR. If the dark current in the detector is diffusion

limited, meaning that the absorber layer thickness is smaller than the diffusion length, then the dark current density scales with the detector dimension.<sup>12</sup>

$$J_{0,diff} = \frac{qn_i^2 d_n}{N_d \tau_p} \tag{1}$$

where  $d_n$  is the absorber layer thickness, q is the electronic charge,  $n_i$  is the intrinsic carrier concentration,  $N_d$  is the concentration of the donor dopant,  $\tau_p$  is the minority carrier lifetime.

While reducing the size of the detector element reduces noise, it also reduces the effective area of the detector that interacts with the incoming infrared radiation. Therefore, in order to realize SNR gain, one must compensate for this loss of signal. Incorporating a resonator antenna has the potential to offset this signal loss. Antennas coupled to infrared detectors can substantially increase quantum efficiency; a recent study showed a quantum efficiency increase by a factor of 3.6 relative to a bare detector. Equation 2 shows how the ratio of noise equivalent power (NEP) for the conventional (bare) and antenna-coupled detectors scales with antenna gain and detector dimension.

$$\frac{NEP(conventional)}{NEP(antenna)} = \frac{\lambda}{b} \left(\frac{g}{4\pi}\right)^{1/2}$$
 (2)

where b is the length of one side of a square detector element and g is the gain of the antenna in the direction of the incident radiation.

Conventional antenna structures are typically metallic. However metals are lossy at LWIR wavelengths, resulting in degraded antenna efficiency. An all-dielectric antenna provides a viable alternative by exploiting displacement currents in the dielectric rather than conduction currents in metal for radiation. In addition, dielectric materials can be patterned using standard photolithography, making them compatible with detector integration. Silicon has very low loss at LWIR wavelengths, thus the efficiency of a silicon-based antenna can be high.

A dielectric resonator coupled with an antimonide detector element function effectively as an antenna and load. Instead of a conventional 50  $\Omega$  load, the detector serves as a load embedded within the antenna, as shown in Figure 1. The antenna is resonant and therefore cancels the reactive power. The relative sizing of the DRA and detector, as well as positioning of the detector within the DRA, allows for optimized impedance matching, which is critical for realizing maximal SNR in the system.

# 3. THEORETICAL SIMULATIONS

A series of numerical simulations were performed to validate the DRACAD concept and to explore design parameters toward development of a demonstration system. Full-wave simulation results were performed to study the LWIR absorption response of single DRACAD element as well as a finite array of elements. As a first step, a model of the DRACAD architecture was developed using the geometry shown in Figure 1 and optical constants for the DRA and detector components. Amorphous silicon was selected to compose the DRA structure, with permittivity  $\epsilon_r = 10.74$  extracted from ellipsometry measurements. For the antimonide detector, the complex index of refraction (n=3.5, k=0.15915) was estimated based on prior measurements from literature.<sup>2</sup> The optical constants and DRACAD geometry were incorporated into a full-wave electromagnetic solver and a variety of simulations were performed to demonstrate detection performance.

Figure 2 shows an example of the calculated detector absorption as a function of wavelength for the cases of a bare detector and an integrated DRACAD structure. The dimensions of the DRA were selected to optimize impedance matching and achieve resonance near a wavelength of 9 µm. The absorption is calculated by forming the ratio of the integral of the loss density within the detector region itself to the incident power density upon the DRACAD. The detector is assumed to be a homogeneous lossy material with loss tangent 0.09113 and dielectric constant of 10.74 taken from the ellipsometry results. As shown in Figure 2, the detector absorption increases from approximately 5% for the bare detector to over 60% for the DRACAD system. This preliminary result indicates that the DRACAD concept has

potential to enhance SNR at LWIR wavelengths and that the performance of the system can be tailored for specific wavelengths based primarily on geometric considerations.

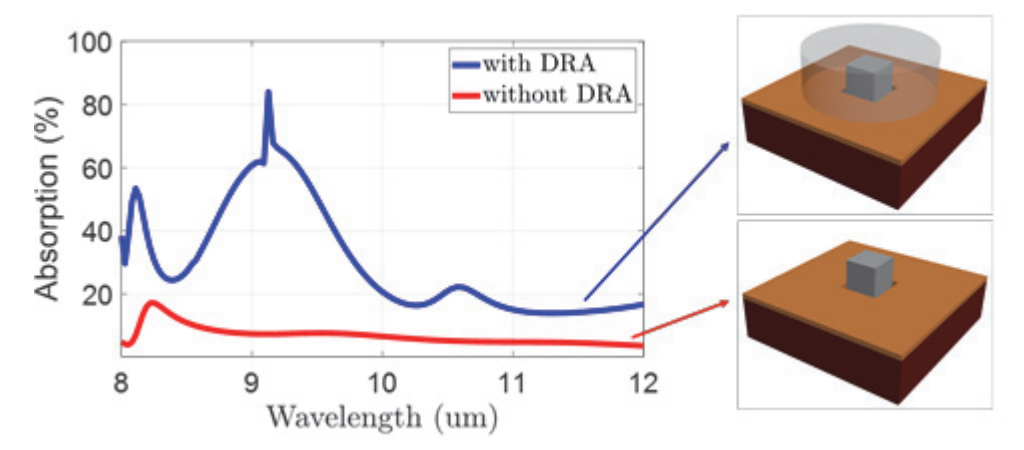


Figure 2. Comparison of theoretical simulations of the optical absorption performance for a single element DRACAD vs. a bare detector with no integrated DRA structure. Absorption is enhanced by a factor of 12 near 9 mm due to the presence of the coupled resonant antenna.

A parametric study was performed to find the optimum dimensions of the DRA, which was then used to compute the absorption performance of a single element and finite array. Additionally, a series of analyses were done to study the absorption sensitivity of the detector to design variables. As shown in Figure 3, the optical performance of the DRACAD is robust with respect to variations of the DRA and detector dimensions.

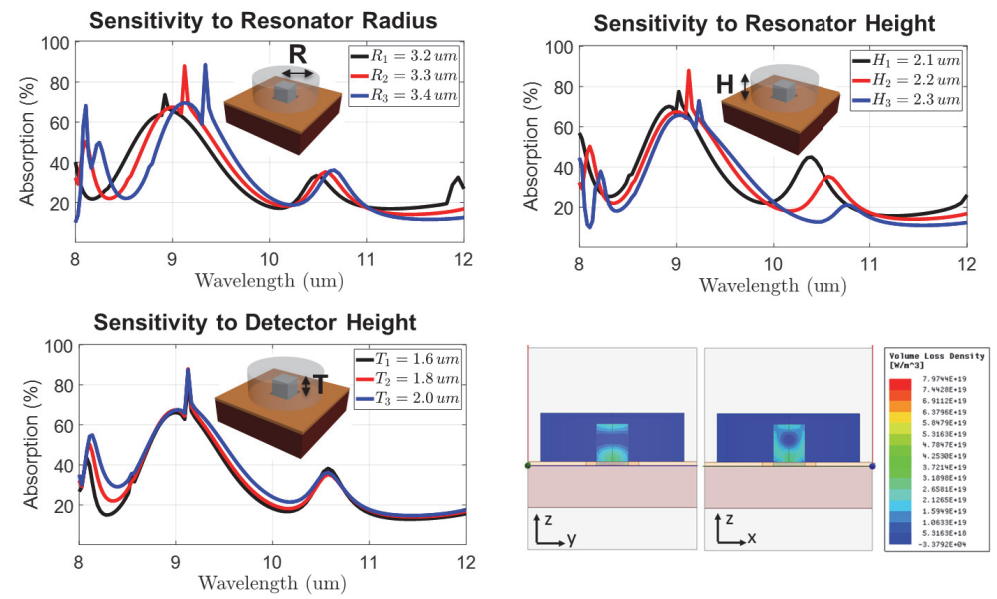


Figure 3. Sensitivity analysis results show that the DRACAD performance is robust with respect to variations in the DRA and detector dimension.

## 4. DEVICE FABRICATION

Based on the results of the numerical simulations and parametric study, an optical test device based on the DRACAD topology was designed and fabricated in order to provide experimental verification of the simulation results. The fabrication process involved epitaxial growth of the antimonide detector, photolithographic etching of the detector material into an array, and  $\alpha$ -Si deposition and deep reactive ion etching to form the DRA structures. A variety of test devices were fabricated for intercomparison, including blanks (ground plane with no detector or DRA), bare detectors (no DRA), DRA structures (no detector), and fully integrated DRACAD structures.

Figure 4 shows a schematic diagram of the design for the InAsSb detector material and the predicted band diagram. The detector material was grown by molecular beam epitaxy and the resultant wafers were characterized by Nomarski imaging, Electron Channel Contrast Imaging (ECCI), and photoluminescence measurements. The material characterization measurements indicated a high quality detector (good metamorphic growth, low threading dislocation density) with a photoluminescence peak at 9 µm.

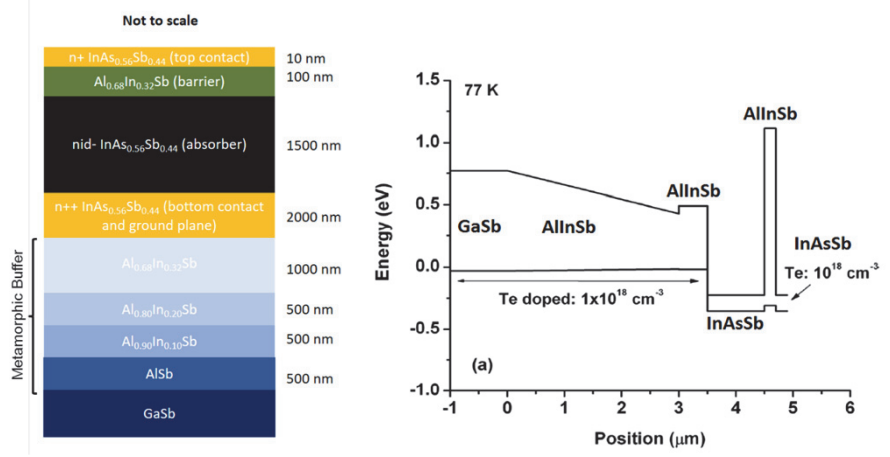


Figure 4. InAsSb superlattice detector design (left) and projected band gap diagram (right).

After receiving the grown InAsSb wafers, a variety of etching processes were explored to produce the individual detector elements needed for the DRACADs. The detector element in the simulated DRACAD was designed to have vertical sidewalls and a disk-shaped antenna. However, the first set of detector mesas produced by inductively couple plasma (ICP) etching with chlorine gas had slanted sidewalls, as observed in scanning electron microscope (SEM) images. The angle formation on the mesa walls are in part due to the lateral component of the ICP etch, which generally can be controlled by adjusting the pressure and DC bias in the chamber. In order to address the slanted sidewalls, we tried using a different etch chemistry with Cl<sub>2</sub>/Ar/H<sub>2</sub> gases. Additionally, a metallic mask made of nickel (Ni) was tested to reduce the charging effect, shown in Figure 5a. As opposed to a PR mask that is an insulator, metal hard masks are conductors and should conduct the charge through the substrate and thus should mitigate the charging effect. While, the new etch recipe with Cl<sub>2</sub>/Ar/H<sub>2</sub> resulted in more vertical sidewalls, the etch rate was slow. The Ni mask and chlorine-based etching led to more vertical sidewalls, but generated 'micro masking' which slowed down the etching rate (Figure 5c). Additional theoretical simulations were performed to assess the impact of the angled sidewalls, and results indicated that significant absorption can still be realized despite the angled geometry. Therefore, slight adjustments were made in the chlorine-based recipe to obtain structures with ~62° sidewalls (Figure 5b). This recipe consistently produced detector mesas with these profile dimensions, and were used for subsequent processing runs.

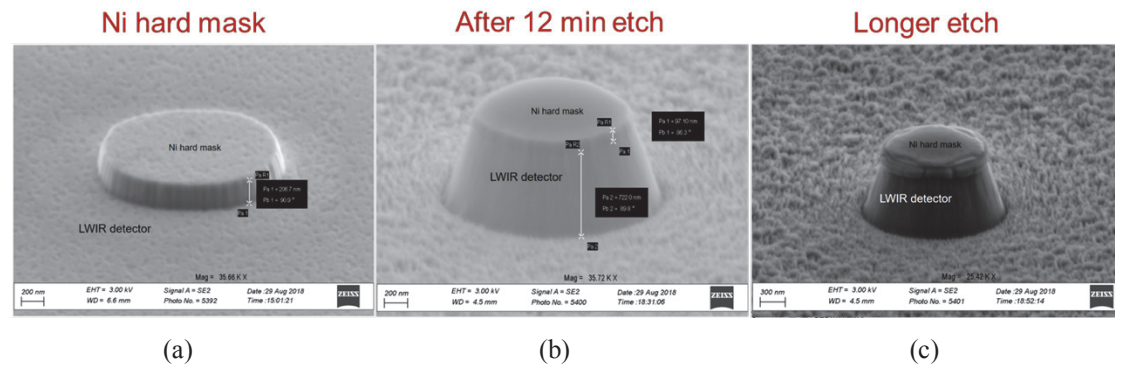


Figure 5. SEM images of the Ni hard mask (a), angled side walls of the resultant detector (b), and micro masking effects due to longer etch times (c).

The DRA elements were fabricated by depositing  $\alpha$ -Si onto the detector mesas using plasma enhanced chemical vapor deposition (PECVD). Figure 6 shows a test sample of  $\alpha$ -Si DRA micro disk arrays deposited on SiO<sub>2</sub>/Si. Subsequent

etching of the micro disks was accomplished using CF4/O2 chemistry. As shown in Figure 6d, a trenching effect was observed near the base of the  $\alpha$ -Si micro disks, which can be controlled by reducing ion density or DC bias.

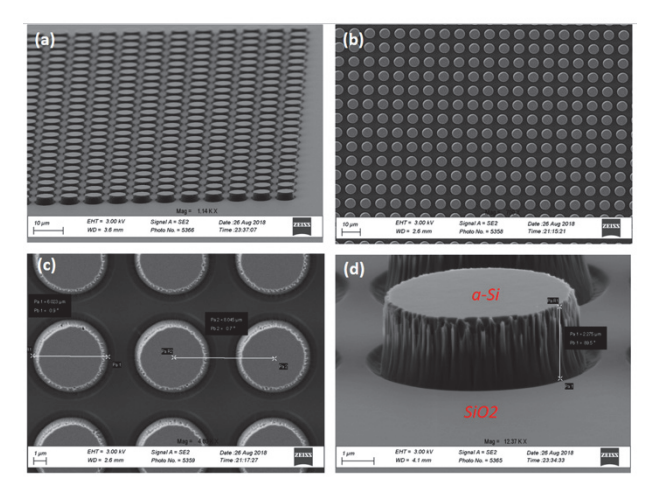


Figure 6. (a) Side view SEM image of  $\alpha$ -Si micro disks patterned on SiO<sub>2</sub>/Si. (b) Top view image of the same patterned structure. (c) Close up top view SEM image showing pitch size of 8  $\mu$ m. (d) Side view SEM image of a single element  $\alpha$ -Si microdisk showing trenching effect due to ion deflection from the photoresist mask.

The final, completed DRACAD elements are shown in Figure 7. The DRA elements exhibit a "bump" on the top that is due to  $\alpha$ -Si material displaced by the detector element during deposition (Figure 7a). The detector element is smaller than the DRA element (Figure 7b), and the bump on top of the DRA directly mimics the detector shape and size. Subsequent numerical simulations were conducted to investigate the impact of the final DRACAD geometry.

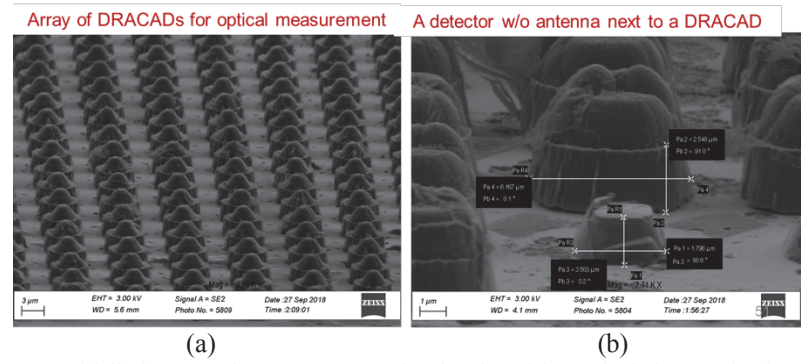


Figure 7. (a) SEM images of fully integrated DRACAD samples developed for optical characterization. (b) Comparison of a DRA coupled detector next to a single detector mesa in a region in which the DRA structure was removed accidently.

# 5. EXPERIMENTAL RESULTS

The optical absorption properties of the DRACAD system were characterized using Fourier transform infrared (FTIR) microscopy (model Thermo Scientific iN5). For each FTIR measurement, a reference spectrum was acquired of a blank sample, which is essentially a gold-plated substrate. Subsequent measurements of bare detectors and DRACAD elements are normalized by the reference spectrum to produce a reflectance spectrum of the sample. The microscope objective is a Cassegrain reflector, which is designed to receive primarily specularly reflected light from the surface of the material under test. If no diffuse reflection or scattering components are present (i.e., smooth surface), then absorption is equal to the quantity (1-reflectance). Figures 8a and 8b shows plots of (1-reflectance) vs. wavelength, indicating that possibility of enhanced absorption in the DRACAD over the 8-12 µm range. However, given the inherent periodicity of the DRACAD samples (8µm) and the fact that the illuminating beam from the Cassegrain reflector is obliquely incident, additional diffracted components are present, as shown in Figure 8c.

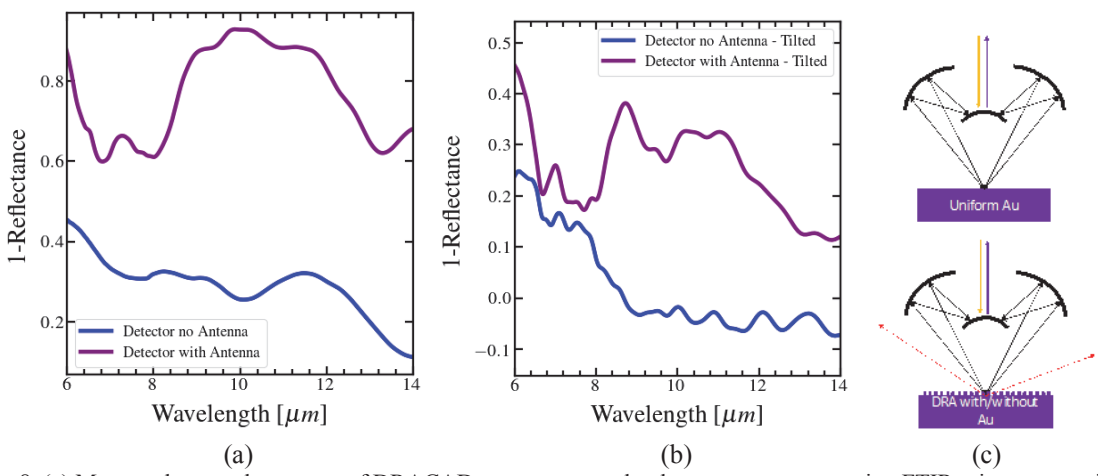


Figure 8. (a) Measured spectral response of DRACAD array compared to bare antenna array using FTIR microscopy with sample at normal incidence to the infrared beam. (b) Same comparison with sample tilted 30° relative to the incident beam. (c) Schematic diagram of the Cassegrain reflector objective, showing the possibility of scattering from the DRACAD samples due to the angle of incidence of the infrared beam not being normal to the DRACAD surface.

These diffracted components are not collected by the Cassegrain objective in general, as the collecting optics are designed to only receive the specularly reflected component within an angular cone of acceptance (19-46° with respect to the normal of the sample). Thus, the light not collected could be due to either absorption or diffracted light not scattered within the acceptance cone. However, the prominent peak of the detector with antenna curve around 9  $\mu$ m, which is the resonant design frequency of the DRA, indicates that absorption could be taking place. In an attempt to compensate for diffraction effects due to the angle of incidence of the infrared beam, the sample plate was tilted 30 degrees relative to its normal configuration, thereby reducing (but not eliminating) any diffraction effects. Figure 8b shows the resulting spectrum from this configuration, indicating that diffraction effects are present in Figure 8a. The figure also shows strong possible absorption at  $9\mu$ m. However, these plots still indicate that increased absorption is occurring in the 8-12  $\mu$ m range and that the DRACAD concept shows significant promise for SNR enhancement in a future LWIR detector device.

## 6. CONCLUSIONS

The work reported here has provided a successful demonstration of the DRACAD concept, both via numerical electromagnetic simulation and preliminary experimental verification. Extensive simulations indicate that the DRACAD concept will provide enhanced infrared absorption and that the geometry can be tailored to produce desired spectral properties. A DRACAD design has been developed, and optical test devices have been fabricated using a variety of deposition and etching processes. Preliminary experimental results verify that enhanced absorption occurs as expected in the LWIR wavelength range. However, the measurements were problematic due to the presence of diffraction, and fully quantifiable results are not yet possible.

Additional work, therefore, is needed to develop an optical characterization setup that can collect all of the light reflected from the DRACAD to provide more accurate measurement of the detector absorption. This may be accomplished by using lenses instead of a Cassegrain reflector or by using an integrating sphere. In addition, a more comprehensive set of experimental data is needed to further validate the simulation results and therefore improve future DRACAD designs. One area of focus will be to consider multiple geometric configurations of the DRA structure in order to broaden the spectral response of the DRACAD beyond individual resonances supported by a simple cylindrical DRA element. In addition, full radiometric testing of an electrical test sample, particularly in a backside illuminated configuration, would provide better insight into a future focal plane array device.

#### REFERENCES

- [1] Montoya, J. A., Tian, Z. B., Krishna, S., Padilla, W. J., "Ultra-thin infrared metamaterial detector for multicolor imaging applications," Optics Express, 25(19), 23343-23355 (2017).
- [2] Wang, S., Yoon, N., Kamboj, A., Petluru, P., Zheng, W. and Wasserman, D., "Ultra-thin enhanced-absorption long-wave infrared detectors," Appl. Phys. Lett. 112(9), 091104 (2018).
- [3] Choi, K. K., Jhabvala, M. D., Sun, J., Jhabvala, C. A., Waczynski, A., and Olver, K., "Resonator-quantum well infrared photodetectors," App. Phys. Lett. 103, 201113 (2013).
- [4] Nolde, J. A., Jackson, E. M., Kim, M., Kim, C. S., Canedy, C. L., Warren, M. V., Tomasulo, S., Affouda, C. A., Cleveland, E. R., Vurgaftman, I., Meyer, J. R., and Aifer, E. H., "Enhancement of quantum efficiency in nBn detectors with thin absorbers using plasmonic gratings," Proc. SPIE 10926, Quantum Sensing and Nano Electronics and Photonics XVI, 1092627 (1 February 2019).
- [5] Peters, D. W., Davids, P. S., Kim, J. K., Leonhardt, D., Beechem, T. E., Howell, S. W., Ohta, T., Wendt, J. R., and Montoya, J. A., "Application to plasmonic subwavelength structuring to enhance infrared detection," Proc. SPIE 8994, Photonic and Phononic Properties of Engineered Nanostructures IV, 899419 (19 February 2014).
- [6] Kroemer, H., "The 6.1A family (InAs, GaSb, AlSb) and its heterostructures: a selective review," Physica E 20(3), 196-203 (2004)
- [7] Rodriguez, J. B., Plis, E., Bishop, G., Sharma, Y. D., Kim, H., Dawson, L. R., Krishna, S., "nBn structure based on InAs/GaSb type-II strained layer superlattices," Appl. Phys. Lett. 91, 043514 (2007).
- [8] Kim, H. S., Plis, E., Rodriguez, J. B., Bishop, G. D., Sharma, Y. D., Dawson, L. R., Krishna, S., Bundas, J., Cook, R., Burrows, D., Dennis, R., Patnaude, K., Reisinger, A., Sundaram, M., "Mid-IR focal plane array based on type-II InAs/GaSb strain layer supperlattic detector with nBn design," Appl. Phys. Lett. 92, 183502 (2008)
- [9] Svensson, S. P., Sarney, W. L., Hier, H., Lin, Y., Wang, D., Donetsky, D., Shterengas, L., Kipshidze, G., and Belenky, G., "Band gap of InAs<sub>1-x</sub>Sb<sub>x</sub> with native lattice constant," Phys. Rev. B 86, 245205 (2012).
- [10] Sarney, W. L., Svensson, S. P., Xu, Y., Donetsky, D., and Belenky, G., "Bulk InAsSb with 0.1 eV bandgap on GaAs," J. Appl. Phys. 112, 025705 (2017).
- [11] Dahiya, V., Deitz, J. I., Hollingshead, D. A., Grassman, T. J., Krishna, S., "Investigation of digital alloyed AlInSb metamorphic buffers," J. Vac. Sci. Tech. B 36, 02D111 (2018).
- [12] Wijewarnasuriya, P. S., "Tutorial on physics of infrared photovoltaic devices," Seminar at The Ohio State University (2018).
- [13] Schwarz, S. E. and Ulrich, B. T., "Antenna-coupled infrared detectors," J. Appl. Phys. 48, 1870 (1977).